

# Thermoelectric properties of in-plane 90<sup>0</sup>-bent graphene nanoribbons with nanopores

Van-Truong Tran<sup>1</sup> and Alessandro Cresti<sup>2</sup>

IMPMC, Université Pierre et Marie Curie (UPMC), Sorbonne Universités, 75252 Paris Cedex 05, France

Univ. Grenoble Alpes, Univ. Savoie Mont Blanc, CNRS, Grenoble INP, IMEP-LAHC, 38000 Grenoble, France

## Abstract

We study the thermoelectric performance of 90<sup>0</sup>-bent graphene nanoribbons containing nanopores for optimized design of multiple functional circuits including thermoelectric generators. We show that the thermal conductance of the 90<sup>0</sup>-bent ribbons is lower from few times to an order of magnitude compared to that of armchair and zigzag straight ribbons. Consequently, the thermoelectric performance of the bent ribbons is better than its straight ribbon counterparts, in particular at high temperature above 500 K. More importantly, the introduction of nanopores in the vertical part of the bent ribbons is demonstrated to strongly enhance their thermoelectric capacity. At 500 K, the figure of merit  $ZT$  increases by more than 160% (from 0.39 without pores to 0.64) with 3 nanopores incorporated, and by more than 200% (up to 0.88) when 24 nanopores are introduced.  $ZT \approx 1$  can be achieved at a temperature of about 1000 K. In addition, the thermoelectric performance is shown to be further improved by combining asymmetrical leads. This study demonstrates that 90<sup>0</sup>-bent ribbons with nanopores have decent thermoelectric performance for a wide range of temperatures and can be used as thermoelectric components in designs of circuits.

## 1. Introduction

Electronics has seen a huge advance over the past half-century thanks to the massive and rapid progress in the downscale size of transistors, which helps to design more compact electronic circuits and therefore smaller devices with higher performance [1]. However, heat management in small electronic devices has been facing many challenges due to very high heat flux that can shorten the lifetime of the device [2,3]. Together with the search for better thermal conductors or efficient designs to dissipate heat in devices, the possibility to harvest

the wasted heat and convert it into electric energy represents an important challenge [4,5], which has inspired the designs of circuits with multiple functions including thermoelectric generators.

Nanostructures based on graphene and other 2D materials have been considered to be potential for making compact and efficient electronic components in circuits thanks to their existence in thin layers and outstanding physical properties [3,6–11]. In particular, although the natural thermoelectric ability of graphene is poor [12], this material is still versatile for thermoelectric applications as its nanostructuration allows the engineering of its electronic and thermal properties and therefore highly tuneable thermoelectric performance [12–16]. In particular, graphene nanoribbons (GNRs) show higher thermoelectric performance compared to 2D sheets thanks to the presence of a band gap that leads to larger Seebeck coefficients [12]. By engineering GNRs with isotopes doping [15], nanopores [17–19], vacancies [20,21], or edge roughness [22–24], it has shown that the thermoelectric performance of GNRs can be tuned in a wide range with the figure of merit  $ZT$  varying from 0.1 to 4.

The best thermoelectric performance of graphene-based systems so far is found in straight ribbons [15,19,22,25]. However, to integrate different systems into a circuit for multiple functions, the arrangement of different components might require the use of bent ribbons to optimize the space in the circuit [26,27]. Due to a strong variation of both electronic and thermal properties of graphene ribbons with the specific edge orientation, the thermoelectric performance of bent ribbons could vary significantly compared to that of straight ones. Although a few works have studied the electronic [28–30], thermal [31,32], and thermoelectric properties of in-plane bent ribbons [33], their level of efficiency in thermoelectric conversion still needs investigation.

In this work, we focus on the improvement of the thermoelectric performance of ribbons bent with an angle of  $90^\circ$ , which exhibits the lowest thermal conductance compared to other angles [31]. To this aim, we introduce nanopores in the bent ribbon systems to further reduce the thermal conductance and optimize the thermoelectric performance. We also consider asymmetrical leads to maximize the mismatch between in-coming and out-going phonon modes for an additional degradation of the phonon conductance and further enhancement of the thermoelectric performance. Our goal is to optimize  $90^\circ$ -bent ribbons to make them suitable as thermoelectric components in multiple functional circuits.

The rest of the paper is organized as follows. In Sec. 2, we describe the studied system, introduce the tight-binding (TB) model for electrons and the Force Constant (FC) model for phonons, and present the Non-Equilibrium Green's Functions (NEGF) formalism for the simulation of transport properties. Section 3 presents and discuss our numerical results. In Sec. 3.1, we focus on the thermoelectric ability of  $90^\circ$ -bent ribbons containing a single nanopore. In Sec. 3.2, we investigate the variation of the electronic, thermal and thermoelectric properties of bent ribbons in the presence of multiple nanopores. In Sec. 3.3, the impact of asymmetrical leads is discussed. Finally, conclusions are given in Sec. 4.

## 2. Studied device and methodology

### 2.1. Studied device

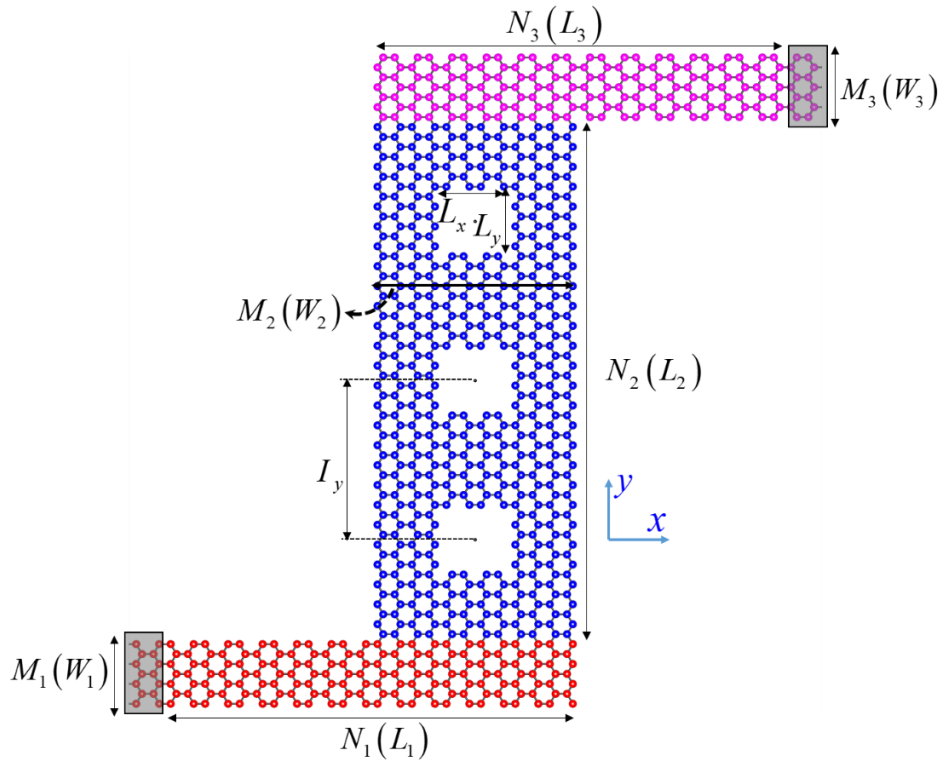


**Fig. 1:** Sketch of a  $90^\circ$ -bent graphene nanoribbon composed of two horizontal armchair-edge sections and a vertical zigzag-edge section. Size of the ribbon parts:  $M_1 = 7$  ( $W_1 \approx 0.74$  nm),  $N_1 = 12$  ( $L_1 \approx 5.11$  nm);  $M_2 = 12$  ( $W_2 \approx 2.41$  nm),  $N_2 = 13$  ( $L_2 \approx 6.39$  nm);  $M_3 = 7$  ( $W_3 \approx 0.74$  nm),  $N_3 = 12$  ( $L_3 \approx 5.11$  nm). Size of nanopores:  $L_x = L_y = 5a_0$ ,  $I_y = 13.86a_0$ ,  $n_{\text{pores}} = 3$ .

A typical device made of a  $90^\circ$ -bent graphene nanoribbon is illustrated in Fig. 1, where the two horizontal segments are made of armchair graphene ribbons (AGNRs) and the vertical

part is a zigzag graphene ribbon (ZGNR). For each section, the size is defined by the width of the ribbon and its length along the ribbon axis. The width of an AGNR section is  $W_A = (M - 1) \times \sqrt{3} / 2 \times a_0$ , and that of a ZGNR section is  $W_Z = (3M - 2) \times a_0 / 2$ , where  $a_0 = 0.142 \text{ nm}$  is the distance between the two nearest carbon atoms and  $M$  is the number of dimer (chain) lines along the ribbon width of an AGNR (ZGNR) [34]. The bottom (top) horizontal ribbon contains  $N_1$  ( $N_3$ ) cells, each composed of 2 slices perpendicular to the  $x$ -axis and with a length  $L_1 = 3 \times a_0 \times N_1$  ( $L_3 = 3 \times a_0 \times N_3$ ). The vertical ribbon is perpendicular to the  $y$ -axis and consists of  $N_2$  cells each composed of 4 slices and this ribbon part has a length  $L_2 = 2\sqrt{3} \times a_0 \times N_2$ . Nanopores are introduced to reduce the phonon conductance. Their shape is rectangular with the size  $L_x, L_y$ . The distance between neighbor nanopores is  $I_y$ . In the structure sketched in Fig. 1, we have  $M_1 = M_3 = 7$  ( $W_1 = W_3 \approx 0.74 \text{ nm}$ ),  $N_1 = N_3 = 12$  ( $L_1 = L_3 \approx 5.11 \text{ nm}$ ),  $M_2 = 12$  ( $W_2 \approx 2.41 \text{ nm}$ ), and  $N_2 = 13$  ( $L_2 \approx 6.39 \text{ nm}$ ). The number of nanopores is  $n_{\text{pores}} = 3$ , each with  $L_x = L_y = 5a_0$ , and distance  $I_y = 13.86a_0$ .

## 2.2. Methodology

To investigate the thermoelectric properties of bent-ribbons, we employed a TB model to describe electrons, an FC to describe phonons, and the NEGF formalism for simulation of the transport properties of both electrons and phonons.

### *Model for electrons*

In the present work, we adopted a TB model with coupling up to the third nearest neighbors (3NN) to describe electrons. The TB Hamiltonian reads:

$$\begin{cases} H_e = \sum_i \varepsilon_i |i\rangle\langle i| - \sum_{i,j \in 1,3\text{NN}} t_{ij} |i\rangle\langle j| \\ s_{ij} = \langle i|j \rangle \end{cases} \quad (1)$$

where  $\varepsilon_i$  is the on-site energy at the  $i$ -th site, and  $t_{ij}$  and  $s_{ij}$  refer to the hopping and overlap parameters between the  $p_z$  orbitals of the carbon atoms at the  $i$ -th and  $j$ -th sites, respectively. The TB parameters were taken from ref. [34] and were optimized for graphene ribbon structures based on a fitting to *ab initio* results of the electronic structure.

### *Model for phonons*

To study phonon properties, an FC model involving up to the four nearest-neighbor couplings was employed, which has been demonstrated to provide a precise reproduction of the phonon

dispersion of graphene obtained by *ab initio* methods and experimental measurements [35]. The secular equation resulting from Newton's second law for phonons can be written as [36,37]:

$$DU = \omega^2 U, \quad (2)$$

where  $U$  is the matrix containing the vibrational amplitudes of all atoms,  $\omega$  is the angular frequency, and  $D$  is the dynamical matrix [36]:

$$D = [D_{3 \times 3}^{ij}] = \begin{cases} -\frac{K_{ij}}{\sqrt{M_i M_j}} & \text{for } j \neq i \\ \sum_{j \neq i} \frac{K_{ij}}{M_i} & \text{for } j = i \end{cases}, \quad (3)$$

with  $M_i$  the mass of  $i$ -th atom, and  $K_{ij}$  the tensor coupling between the  $i$ -th and  $j$ -th atoms defined by a unitary rotation in the plane:

$$K_{ij} = U^{-1}(\theta_{ij}) K_{ij}^0 U(\theta_{ij}), \quad (4)$$

where  $U(\theta_{ij})$  is the rotation matrix [37],  $\theta_{ij}$  is the angle between the positive direction of the  $x$ -axis and the vector from the  $i$ -th atom to the  $j$ -th atom,  $K_{ij}^0$  is the force constant tensor given by:

$$K_{ij}^0 = \begin{pmatrix} \Phi_r & 0 & 0 \\ 0 & \Phi_t & 0 \\ 0 & 0 & \Phi_{t_o} \end{pmatrix}, \quad (5)$$

where  $\Phi_r, \Phi_t, \Phi_{t_o}$  are the coupling components in radial, transverse in-plane and out-plane, respectively, and they are given parameters of the FC model. In total, we need 12 constant parameters, whose values were taken from Wirtz's work [35]. The mass of carbon atoms is  $1.994 \times 10^{-26}$  kg.

### ***Transport properties***

To investigate the transport properties of both electrons and phonons, we employed the NEGF technique [38]. All structures were considered as composed of three parts: the left and right leads and the device region (central region). The leads were considered as semi-infinite

periodic regions, with the same unit cell as that of the two horizontal ribbons. The device (central) region contains the two horizontal ribbons and the vertical part.

The retarded Green's functions for electrons can be written as:

$$G = \left[ E^+ \cdot S_D - H_D - \Sigma_L^s - \Sigma_R^s \right]^{-1}, \quad (6)$$

where  $E^+ = E + i\eta$  with  $E$  the energy and  $\eta$  is a positive infinitesimal number and

$$\begin{aligned} \Sigma_L^s &= (E^+ \cdot S_{DL} - H_{DL}) G_L^0 (E^+ \cdot S_{LD} - H_{LD}) \\ \Sigma_R^s &= (E^+ \cdot S_{DR} - H_{DR}) G_R^0 (E^+ \cdot S_{RD} - H_{RD}) \end{aligned} \quad (7)$$

are the surface self-energies contributed from the left and right contacts.  $G_{L(R)}^0$  is the surface Green's function of the isolated left (right) contact. To calculate the self-energy, a modification of Sancho-Rubio iterative technique to include the overlap factor was adopted [39,40].

For the phonon calculation, we employed a similar method obtained just by replacing the energy  $E$  by  $\omega^2$ , and  $H_D, H_{DL}, H_{LD}, H_{DR}, H_{RD}$  by  $D_D, D_{DL}, D_{LD}, D_{DR}, D_{RD}$ , respectively. We also considered that  $S_D = \mathbf{1}, S_{DL} = S_{LD} = S_{DR} = S_{RD} = \mathbf{0}$  for phonons.

The recursive technique of ref. [41,42] was employed to efficiently manage the size of the device in the Green's function calculation. Then electrons (phonons) transmission was computed as [36,38]:

$$T_{e(p)} = \text{Trace} \left\{ \Gamma_L^s \left[ i(G_{11} - G_{11}^\dagger) - G_{11} \Gamma_L^s G_{11}^\dagger \right] \right\}, \quad (8)$$

where  $\Gamma_{L(R)}^s = i(\Sigma_{L(R)}^s - \Sigma_{L(R)}^{s\dagger})$  is the surface injection rate at the left (right) contact. The electrical conductance  $G_e$ , the Seebeck coefficient  $S$ , the electron thermal conductance  $K_e$  at given chemical potential  $\mu$  were computed with the Landauer-Onsager's approach [43], i.e.,

$$\begin{aligned} G_e(\mu, T) &= e^2 L_0(\mu, T) \\ S(\mu, T) &= \frac{1}{e} \frac{1}{T} \frac{L_1(\mu, T)}{L_0(\mu, T)} \\ K_e(\mu, T) &= \frac{1}{T} \left[ L_2(\mu, T) - \frac{L_1(\mu, T)^2}{L_0(\mu, T)} \right] \end{aligned} \quad (9)$$

where the intermediate functions  $L_n$  are defined by [36]

$$L_n(\mu, T) = \frac{1}{h} \int_{-\infty}^{+\infty} dE T_e(E) (2k_B T)^{n-1} g_n^e(E, \mu, T), \quad (10)$$

where  $g_n^e(E, \mu, T) = \left( \frac{E - \mu}{2k_B T} \right)^n / \cosh^2 \left( \frac{E - \mu}{2k_B T} \right)$  is a dimensionless function.

The phonon conductance  $K_p$  was computed by [36]

$$K_p = \frac{K_b}{2\pi} \int_0^\infty d\omega \Gamma_p(\omega) g^p(\omega, T), \quad (11)$$

where  $g^p(\omega, T) = \left( \frac{\hbar\omega}{2k_B T} \right)^2 / \sinh^2 \left( \frac{\hbar\omega}{2k_B T} \right)$  and  $k_B$  is the Boltzmann constant. Since the phonon conductance is mainly limited by the extremely reduced size of the bent ribbon, the bending itself, and the presence of nanopores, we can reasonably disregard anharmonic phonon-phonon scattering, which is not included in our model.

The figure of merit  $ZT$  was calculated from the electrical conductance, the Seebeck coefficient, the electron and phonon thermal conductances as [12,36,44]

$$ZT = \frac{G_e S^2}{K_e + K_p} T. \quad (12)$$

### 3. Results and discussions

In this section, first the electronic, thermal and thermoelectric properties of the bent ribbon without and with a single nanopore are compared with those of straight ribbons. Then, additional nanopores are introduced in the system to further enhance phonon scattering. Finally, the role of asymmetrical leads on the thermoelectric performance of bent ribbons is discussed.

#### 3.1. 90°-bent ribbons with a single nanopore

First, we examine the thermal, electronic and thermoelectric properties of bent-ribbons without and with a single nanopore.

As can be observed in Fig. 2(a), the phonon conductance of the bent-ribbon structures (red and blue lines) is about an order of magnitude lower than that of the straight ZGNR, and a few times smaller than that of the straight AGNR. At 500 K, the conductance of the

considered straight zigzag ( $M = 12$ ), armchair ( $M = 7$ ) and the  $90^\circ$ -bent ribbons without and with a square pore with  $L_x = L_y = 5a_0$  is 5.89, 1.63, 0.71, 0.53 nW/K, respectively.

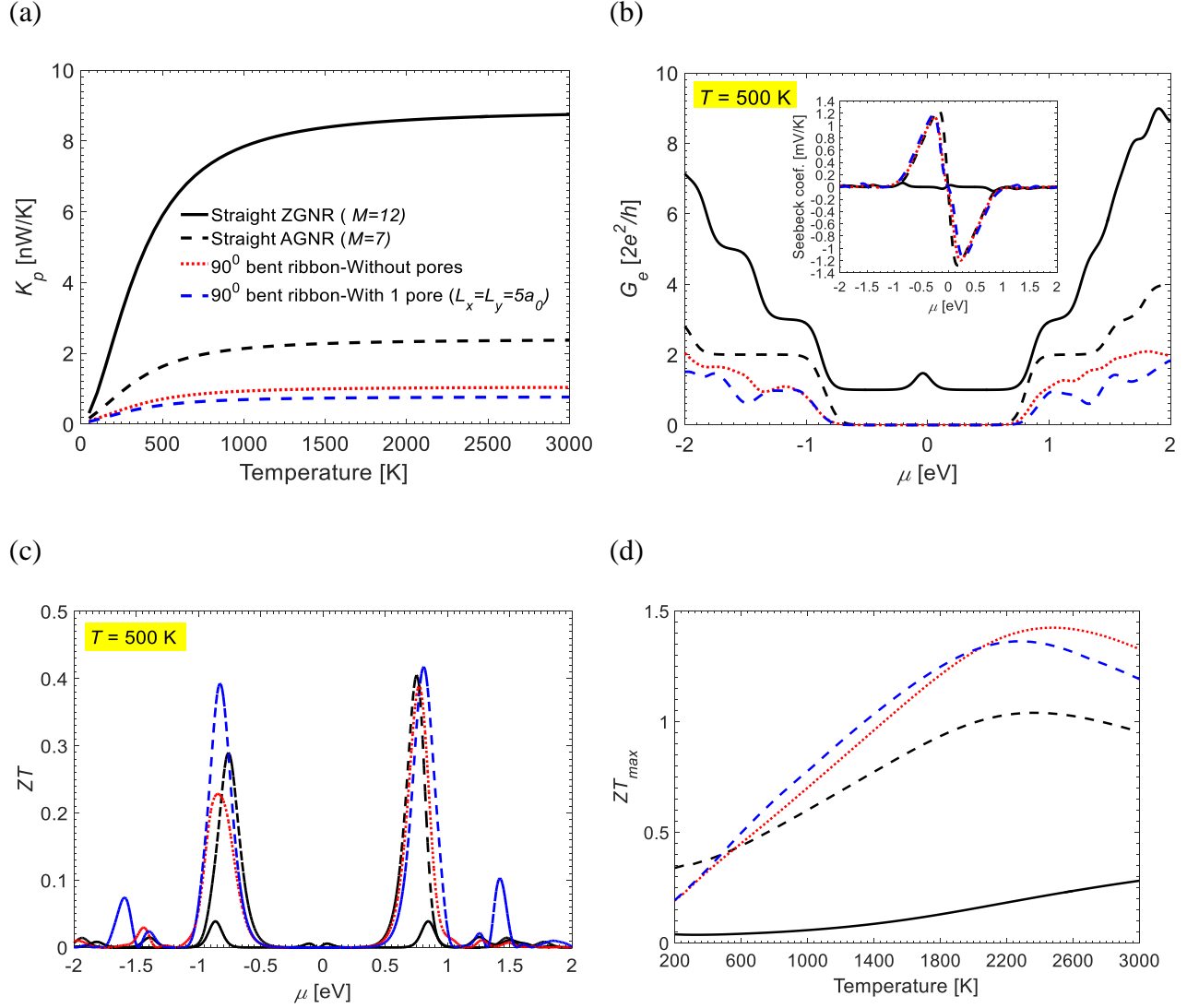


**Fig 2:** (a) Phonon conductance, (b) electrical conductance, (c)  $ZT$  at 500 K as a function of chemical potential, (d)  $ZT_{\max}$  as a function of temperature of the bent ribbon without (red) and with (blue) a nanopore in comparison with those of straight the ZGNR (solid black) and the AGNR (dashed black). The inset in Fig. 2(b) presents the Seebeck coefficient of the four structures. Size of the bent ribbons:  $M_1 = M_3 = 7$  ( $W_1 = W_3 \approx 0.74$  nm),  $N_1 = N_3 = 12$  ( $L_1 = L_3 \approx 5.11$  nm);  $M_2 = 12$  ( $W_2 \approx 2.41$  nm),  $N_2 = 7$  ( $L_2 \approx 3.44$  nm). Size of the nanopore:  $L_x = L_y = 5a_0$ ,  $n_{\text{pores}} = 1$ .

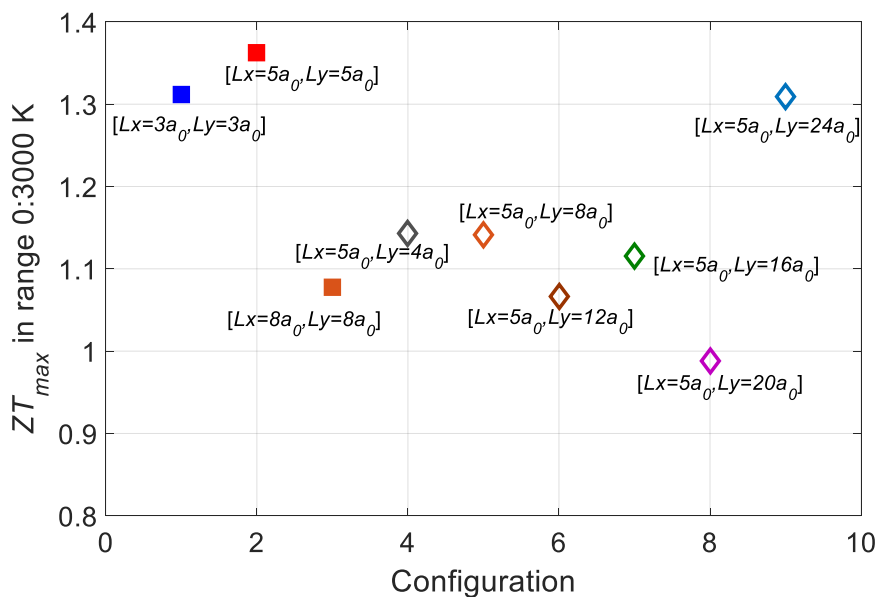


Figure 2(b) presents the electrical conductance and Seebeck coefficient (inset) as a function of the chemical potential  $\mu$  at 500 K of the four studied systems. Due to the semi-metallic behavior, indicated by the non-zero electronic conductance over the whole range of energy, the straight zigzag structure has a very small Seebeck coefficient (see the black solid line in the inset) below  $66 \mu\text{V/K}$ . In contrast, the armchair structure  $M = 7$  and the bent ribbon counterparts all present a decent gap in the electric conductance. Despite change in the direction along the ribbon axis, which causes scattering (for both electrons and phonons) in the systems and a degradation of the electric conductance, the transport gap in these bent structures is observed to be similar to that of the straight AGNR. As a result, the Seebeck coefficient of these bent structures is similar to that of the corresponding straight AGNRs, as shown in the inset of Fig. 2(b). Therefore, the thermoelectric ability of these structures depends on the compromise between the electrical and thermal conductance.

In Fig. 2(c), the figure of merit  $ZT$  at 500 K as a function of chemical potential is shown. Due to the small Seebeck coefficient, the straight ZGNR has a  $ZT$  smaller than 0.04. The maximum  $ZT_{\text{max}}$  of the straight AGNR, the bent-ribbon without and with a square nanopore is 0.41, 0.39 and 0.42, respectively and can be obtained for  $\mu < 1 \text{ eV}$ .

At high temperatures, the  $ZT_{\text{max}}$  is significantly higher for bent ribbons than for straight ribbons, as seen in Fig. 2(d). For example, at 1400 K, the straight ZGNR has  $ZT_{\text{max}} \approx 0.09$ , while this value is about 0.77, 0.96 and 1.03 for the straight AGNR and the bent ribbons without and with the pore, respectively. The effect is even more pronounced at higher temperatures. It is worth mentioning that below 2000 K, the bent ribbon with the nanopore always exhibits better thermoelectric performance than that without pore. This is because of the lower thermal conductance as observed in Fig. 2(a).

To explore the dependence of the thermoelectric ability of the bent ribbon on the shape of the nanopore, the different pore sizes were considered. The  $ZT_{\text{max}}$  as a function of temperature and for different pore sizes is shown in Fig. 3. As can be observed, the size of the nanopore remarkably influences the thermoelectric performance of the bent-ribbons and, among the considered configurations, the ribbon with the square pore with the size  $L_x = L_y = 5a_0$  provides the best  $ZT_{\text{max}} \approx 1.36$ . It is worth noting that other configurations can also have  $ZT_{\text{max}}$  larger than 1.



**Fig. 3:**  $ZT_{\max}$  in a wide range of temperature from 0 to 3000 K for different nanopore sizes. Size of the bent ribbons:  $M_1 = M_3 = 7$  ( $W_1 = W_3 \approx 0.74$  nm),  $N_1 = N_3 = 12$  ( $L_1 = L_3 \approx 5.11$  nm);  $M_2 = 12$  ( $W_2 \approx 2.41$  nm),  $N_2 = 7$  ( $L_2 \approx 3.44$  nm). Only one nanopore is present.

### 3.2. 90<sup>0</sup>-bent ribbons with multiple nanopores

In this section, the effect of multiple nanopores in the vertical part of the bent ribbons is examined as a function of their size and distance  $I_y$ .

In Fig. 4(a), the phonon conductance of the bent ribbons containing 3 nanopores is shown. Different square pore sizes and two cases of the  $I_y$  parameter are considered. The phonon conductance does not change significantly with  $I_y$ , but it does with the pore size. In general, for same  $I_y$ , the thermal conductance is smaller for larger nanopores. The slight difference between configurations with different  $I_y$  could originate from the phonon coherence in ring-like structures, where constructive or destructive phonon interference could occur [45]. Such an interference is even more pronounced in the case of electrons and is commonly referred to as quantum interference [46]. The  $ZT_{\max}$  of these structures is shown in Fig. 4(b) as a function of temperature. Although the structures with the largest pore considered here have a lower phonon conductance, the  $ZT_{\max}$  is found higher for an intermediate pore size. This is because good thermoelectrics requires a compromise between phonon and electron transport properties. Indeed, scatterers that strongly reduce the thermal conductance, commonly also significantly reduce the electronic conductance, which requires a trade-off of the electrical

and thermal contributions for the optimization of the thermoelectric performance. It can also be seen that  $ZT_{\max}$  is higher for nanopores with  $L_x = L_y = 5a_0$  for a wide range of temperature, from room temperature up to about 2000 K.

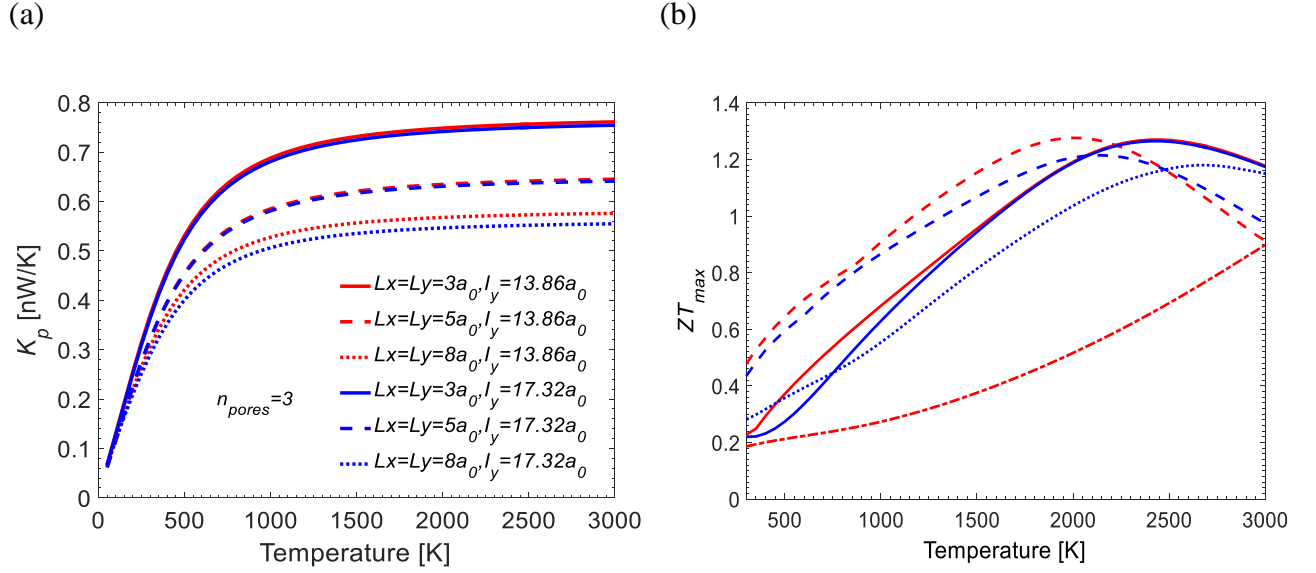


**Fig 4:** (a) Phonon thermal conductance, (b)  $ZT_{\max}$  as a function of temperature for different square nanopores at distance  $I_y$ . The studied structures contain 3 nanopores. Size of the bent ribbons:  $M_1 = M_3 = 7$  ( $W_1 = W_3 \approx 0.74$  nm),  $N_1 = N_3 = 12$  ( $L_1 = L_3 \approx 5.11$  nm);  $M_2 = 12$  ( $W_2 \approx 2.41$  nm),  $N_2 = 13$  ( $L_2 \approx 6.39$  nm).

To see how the thermoelectric performance could be impacted by varying the number of nanopores  $n_{\text{pores}}$  in the vertical part, we considered different length of the vertical ZGNR section. Figure 5(a) shows the corresponding  $ZT_{\max}$  as a function of temperature. The thermoelectric performance for temperature below 1000 K is overall enhanced when increasing  $n_{\text{pores}}$ . A figure of merit  $ZT$  of about 1.4 can be achieved with the structure containing  $n_{\text{pores}} = 12$  at about 2000 K. In Fig. 5(b),  $ZT_{\max}$  is plotted as a function of the number of pores at 300 K (diamonds), 500 K (squares) and 1000 K (triangular), together with its maximum value obtained in the range of temperature from 0 to 3000 K (circles). The results indicate that  $ZT_{\max}$  below 1000 K is enhanced significantly from  $n_{\text{pores}} = 0$  to  $n_{\text{pores}} = 3$ , then it increases gradually and eventually tends to saturate. At 300 K,  $ZT_{\max}$  can be enhanced about 1.85 times from 0.26 without pores to 0.48 with  $n_{\text{pores}} = 3$ , and  $ZT_{\max}$  reaches to 0.69

with  $n_{\text{pores}} = 24$ .  $ZT_{\text{max}}$  at 500 K also increases remarkably from 0.39 without pores to 0.64, 0.71, 0.76 and 0.88 with  $n_{\text{pores}} = 3, 6, 12,$  and 24, respectively.

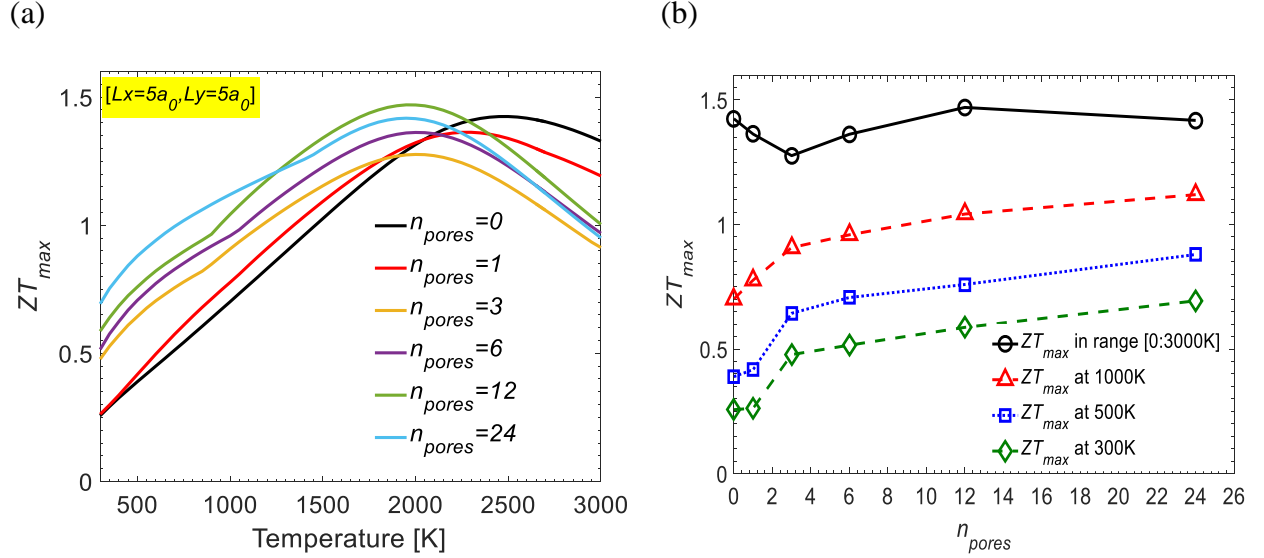


**Fig. 5:** (a)  $ZT_{\text{max}}$  as a function of temperature with different number of nanopores incorporated in the systems. (b)  $ZT_{\text{max}}$  as a function of the number of nanopores at different temperatures. The pore size is fixed for all the structures  $L_x = L_y = 5a_0$ . The size of the bent ribbons:  $M_1 = M_3 = 7$  ( $W_1 = W_3 \approx 0.74$  nm),  $N_1 = N_3 = 12$  ( $L_1 = L_3 \approx 5.11$  nm);  $M_2 = 12$  ( $W_2 \approx 2.41$  nm),  $N_2(L_2)$  varies with the number of nanopores.

It is worth noting that the electronic properties of AGNRs are classified into 3 groups  $3p$ ,  $3p+1$ ,  $3p+2$  with  $p$  in an integer number [47]. On the other hand, the transport gap of the bent ribbons without and with nanopores is directly related to the transport gap of the armchair section, as seen in Fig. 2(b). It is, therefore, worth investigating the dependence of the thermoelectric capacity of bent ribbons on each group of armchair ribbons.

In Fig. 6(a),  $ZT$  at 500 K is plotted as a function of chemical potential for three ribbons of width  $M_1 = M_3 = 7, 8$  and 9 that represent the  $3p+1, 3p+2, 3p$  groups, respectively.  $ZT$  clearly shows the highest peak with the structure of width  $M = 7$  (group  $3p+1$ ). This result can be understood from the fact that the  $3p+1$  group provides the largest band gap [47]. Interestingly, although the  $3p+2$  group has been demonstrated to have the smallest gap among the three groups, the thermoelectric performance of the system with  $M = 8$  turns out to be better than for the system with  $M = 9$  (group  $3p$ ). This indicates that the trade-off between the electrical

conductance and the Seebeck coefficient around the Fermi level is better in the structure with AGNR sections of the  $3p+2$  group than the  $3p$  one.

Figure 6(b) also reports the  $ZT_{\max}$  in a wide range of temperatures from 0 to 3000 K for different structures of these three AGNR groups. The result confirms that the  $3p+1$  group provides higher thermoelectric performance compared to the other groups.

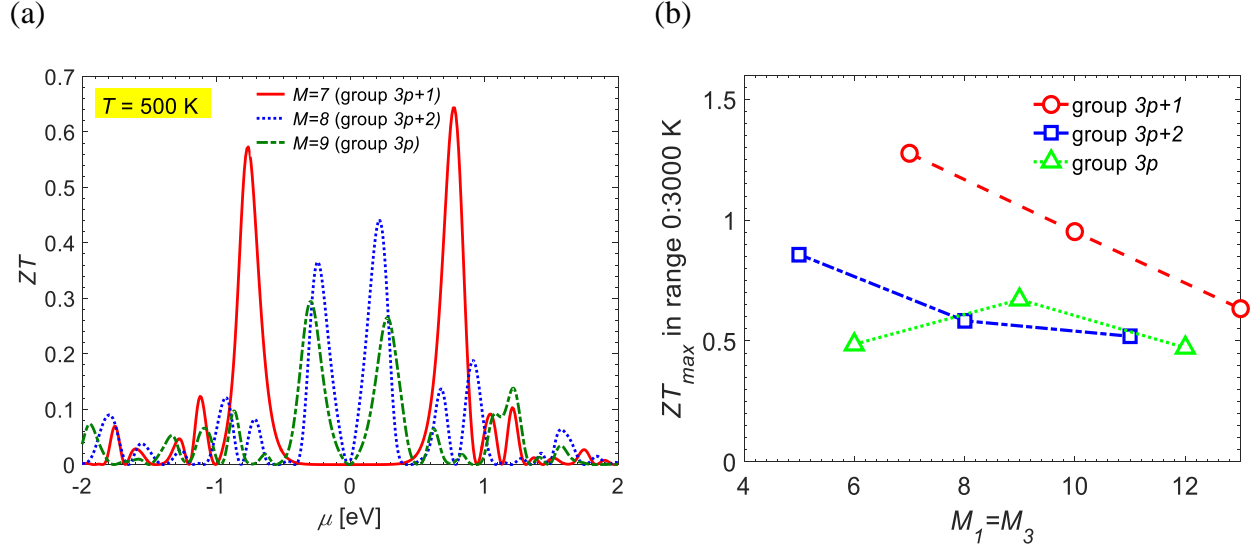


**Fig. 6:** (a)  $ZT$  at 500 K as a function of chemical potential for different armchair ribbons of width used for the horizontal segments, here  $M = M_1 = M_3$ . (b)  $ZT_{\max}$  in a wide range of temperature from 0 to 3000 K is considered for several structures of the three groups  $3p$ ,  $3p+1$ , and  $3p+2$ . Other parameters:  $N_1 = N_3 = 12$  ( $L_1 = L_3 \approx 5.11$  nm);  $M_2 = 12$  ( $W_2 \approx 2.41$  nm),  $N_2 = 13$  ( $L_2 \approx 6.39$  nm),  $L_x = L_y = 5a_0$ ,  $I_y = 13.86a_0$ ,  $n_{\text{pores}} = 3$ .

### 3.3. Asymmetrical leads

All the above structures were considered with symmetrical leads, i.e., with the same width of the lower and upper horizontal ribbons. It might also worth investigating structures with asymmetrical leads, as this can induce further phonon mode mismatch for in-coming and out-going phonon modes in the two leads, and thus a possible higher thermoelectric performance due to a lower thermal conductance.

In Fig. 7(a),  $ZT_{\max}$  is shown for several structures with different pairs of widths  $[M_1, M_3]$  as a function of temperature. For all the considered configurations, three nanopores were introduced. The results reveal that the correlation between the sizes of the two leads strongly

impacts the thermoelectric performance of the systems. Among the considered structures, that with the two leads of width  $M_1 = 7$  and  $M_3 = 11$  exhibits the highest figure of merit  $ZT$ .

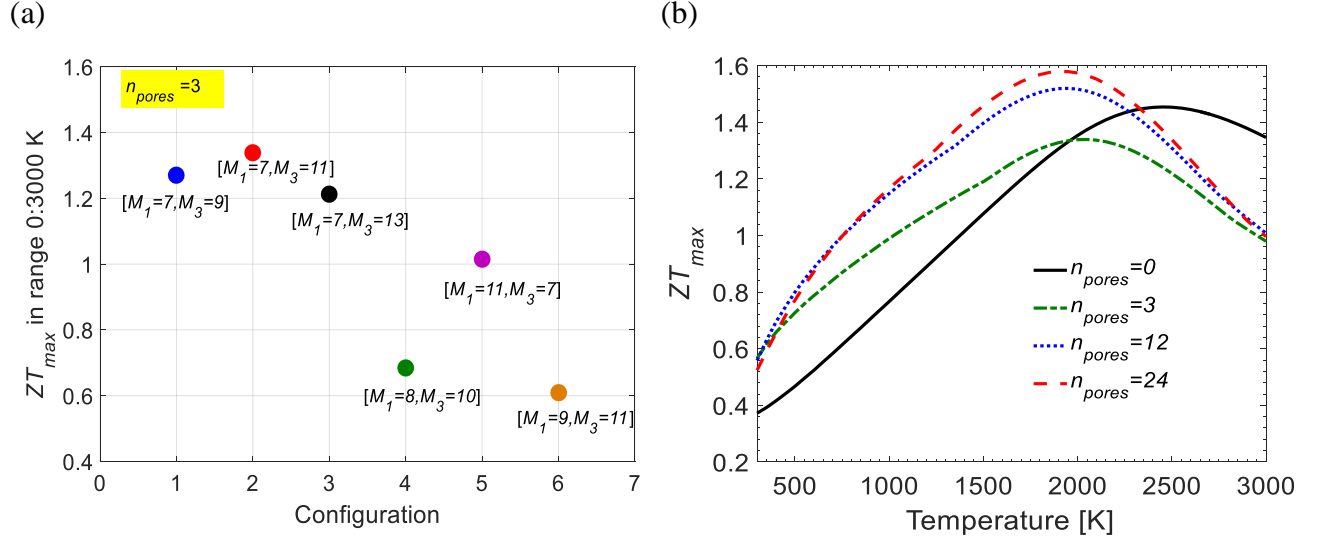


**Fig. 7:** Asymmetrical lead structures: (a)  $ZT_{\max}$  in a wide range of temperatures from 0 to 3000 K is considered for different configurations of asymmetrical leads. All the structures contain 3 nanopores. (b)  $ZT_{\max}$  in structures with  $M_1 = 7, M_3 = 11$  is plotted as a function of temperature for different numbers of nanopores incorporated in the systems. In all structures, nanopores have the size  $L_x = L_y = 5a_0, I_y = 13.86a_0$  and the width of the vertical ribbon is fixed at  $M_2 = 12$  ( $W_2 \approx 2.41$  nm). Other information:  $N_1 = N_3 = 12$  ( $L_1 = L_3 \approx 5.11$  nm).

Further examination for the asymmetrical lead structures with  $M_1 = 7, M_3 = 11, ZT_{\max}$  as a function of temperature for different numbers of incorporated nanopores is shown in Fig. 7(b). As can be observed,  $ZT_{\max} \approx 1.6$  could be reached with asymmetrical lead systems with  $n_{\text{pores}} = 24$  and thus more efficient than the symmetrical lead systems as seen in Fig. 5(a). Compared to the asymmetrical lead system without nanopores (solid black line), the introduction of nanopores significantly increases  $ZT_{\max}$  for a wide range of temperature, for example, at 500 K,  $ZT_{\max}$  increases from 0.46 with  $n_{\text{pores}} = 0$  to 0.73 and 0.78 for  $n_{\text{pores}} = 3$  and 24, respectively.

#### 4. Conclusion

We studied the thermoelectric performance of  $90^\circ$ -bent graphene nanoribbons. The phonon conductance of the bent ribbon turned out to be about an order of magnitude smaller than that

of straight zigzag ribbons and a few times smaller than that of straight armchair ribbons. The electronic transport gap was found to be equivalent to the band gap of the armchair section. However, the electrical conductance showed a slight decrease around the transition region of the first step. Due to such electronic and thermal characteristics, the thermoelectric of the bent ribbon resulted remarkably higher than that of the zigzag ribbon and significantly enhanced compared to the armchair ribbon, in particular above 500 K. By introducing nanopores in the bent structures, the thermoelectric performance was further enhanced thanks to the reduction of the phonon conductance. At 500 K, the  $ZT$  of the bent ribbon increased from 0.39 without nanopores to 0.64, 0.71, 0.76 and 0.88 with 3, 6, 12, and 24 nanopores present in the system, respectively.  $ZT$  above 1 could be achieved at a temperature of about 1000 K and it was observed to become even larger at higher temperatures. According to the analysis of the dependence of the thermoelectric performance for the different groups of armchair ribbons, the highest  $ZT$  turn out to be for the  $3p+1$  group. Finally, the thermoelectric performance was shown to be further improved by combining asymmetrical leads. For example, with two different leads of width  $M_1 = 7$  and  $M_3 = 11$ , the  $ZT$  at 500 K could reach 0.73 even with only 3 nanopores present in the structure. Our results provide an insight into the thermoelectric capacity of  $90^\circ$ -bent graphene ribbons and pave the way to enhance their thermoelectric performance by including nanopores in the structure.

## References

- [1] Schwierz F 2010 Graphene transistors *Nat. Nanotechnol.* **5** 487–96
- [2] Akinwande D, Huyghebaert C, Wang C-H, Serna M I, Goossens S, Li L-J, Wong H-S P and Koppens F H L 2019 Graphene and two-dimensional materials for silicon technology *Nature* **573** 507–18
- [3] Fu Y, Hansson J, Liu Y, Chen S, Zehri A, Samani M K, Wang N, Ni Y, Zhang Y, Zhang Z-B Bin, Wang Q, Li M, Lu H, Sledzinska M, Torres C M S S, Volz S, Balandin A A, Xu X and Liu J 2020 Graphene related materials for thermal management *2D Mater.* **7** 012001
- [4] Zheng X F, Liu C X, Yan Y Y and Wang Q 2014 A review of thermoelectrics research - Recent developments and potentials for sustainable and renewable energy applications *Renew. Sustain. Energy Rev.* **32** 486–503
- [5] Beretta D, Neophytou N, Hodges J M, Kanatzidis M G, Narducci D, Martin-Gonzalez M, Beekman M, Balke B, Cerretti G, Tremel W, Zevalkink A, Hofmann A I, Müller C, Dörling B, Campoy-Quiles M and Caironi M 2019 Thermoelectrics: From history, a window to the future *Mater. Sci. Eng. R Reports* **138** 210–55
- [6] Schwierz F, Pezoldt J and Granzner R 2015 Two-dimensional materials and their prospects in transistor electronics *Nanoscale* **7** 8261–83
- [7] Marmolejo-Tejada J M and Velasco-Medina J 2016 Review on graphene nanoribbon

- devices for logic applications *Microelectronics J.* **48** 18–38
- [8] Liu Y, Weiss N O, Duan X, Cheng H-C, Huang Y and Duan X 2016 Van der Waals heterostructures and devices *Nat. Rev. Mater.* **1** 16042
- [9] Novoselov K S, Fal'ko V I, Colombo L, Gellert P R, Schwab M G and Kim K 2012 A roadmap for graphene *Nature* **490** 192–200
- [10] Pop E, Varshney V and Roy A K 2012 Thermal properties of graphene: Fundamentals and applications *MRS Bull.* **37** 1273–81
- [11] Lin X, Yang W, Wang K L and Zhao W 2019 Two-dimensional spintronics for low-power electronics *Nat. Electron.* **2** 274–83
- [12] Dollfus P, Nguyen V H, Saint-Martin J, Hung Nguyen V, Saint-Martin J, Nguyen V H and Saint-Martin J 2015 Thermoelectric effects in graphene nanostructures *J. Phys. Condens. Matter* **27** 133204
- [13] Kim J Y and Grossman J C 2015 High-efficiency thermoelectrics with functionalized graphene *Nano Lett.* **15** 2830–5
- [14] Yan Y, Liang Q F, Zhao H, Wu C Q and Li B 2012 Thermoelectric properties of one-dimensional graphene antidot arrays *Phys. Lett. Sect. A Gen. At. Solid State Phys.* **376** 2425–9
- [15] Tran V-T, Saint-Martin J, Dollfus P and Volz S 2017 Optimizing the thermoelectric performance of graphene nano-ribbons without degrading the electronic properties *Sci. Rep.* **7** 2313
- [16] Haskins J, Kinaci A, Sevik C, Sevincli H, Cuniberti G and Cagin T 2011 Control of thermal and electronic transport in defect-engineered graphene nanoribbons *ACS Nano* **5** 3779–87
- [17] Chang P H and Nikolić B K 2012 Edge currents and nanopore arrays in zigzag and chiral graphene nanoribbons as a route toward high-ZT thermoelectrics *Phys. Rev. B - Condens. Matter Mater. Phys.* **86** 1–5
- [18] Sadeghi H, Sangtarash S and Lambert C J 2015 Enhanced Thermoelectric Efficiency of Porous Silicene Nanoribbons *Sci. Rep.* **5** 1–7
- [19] Chang P H, Bahramy M S, Nagaosa N and Nikolić B K 2014 Giant thermoelectric effect in graphene-based topological insulators with heavy adatoms and nanopores *Nano Lett.* **14** 3779–84
- [20] Mazzamuto F, Saint-Martin J, Nguyen V H, Chassat C and Dollfus P 2012 Thermoelectric performance of disordered and nanostructured graphene ribbons using Green's function method *J. Comput. Electron.* **11** 67–77
- [21] An R L, Wang X F, Vasilopoulos P, Liu Y S, Chen A B, Dong Y J and Zhai M X 2014 Vacancy effects on electric and thermoelectric properties of zigzag silicene nanoribbons *J. Phys. Chem. C* **118** 21339–46
- [22] Sevincli H, Cuniberti G, Sevincli H, Cuniberti G, Sevincli H, Cuniberti G, Sevincli H and Cuniberti G 2010 Enhanced thermoelectric figure of merit in edge disordered zigzag graphene nanoribbons *Phys. Rev. B* **81** 4
- [23] Hossain M S, Huynh D H, Nguyen P D, Jiang L, Nguyen T C, Al-Dirini F, Hossain F M and Skafidas E 2016 Enhanced thermoelectric performance of graphene nanoribbon-based devices *J. Appl. Phys.* **119**



- [24] Karamitaheri H, Pourfath M, Faez R and Kosina H 2013 Atomistic study of the lattice thermal conductivity of rough graphene nanoribbons *IEEE Trans. Electron Devices* **60** 2142–7
- [25] Hossain M S, Al-Dirini F, Hossain F M and Skafidas E 2015 High Performance Graphene Nano-ribbon Thermoelectric Devices by Incorporation and Dimensional Tuning of Nanopores *Sci. Rep.* **5** 1–12
- [26] Kang J, Sarkar D, Khatami Y and Banerjee K 2013 Proposal for all-graphene monolithic logic circuits *Appl. Phys. Lett.* **103** 083113
- [27] Liu C, Yao B, Dong T, Ma H, Zhang S, Wang J, Xu J, Shi Y, Chen K, Gao L and Yu L 2019 Highly stretchable graphene nanoribbon springs by programmable nanowire lithography *npj 2D Mater. Appl.* **3** 23
- [28] Wang Z F, Li Q, Shi Q W, Wang X, Hou J G, Zheng H and Chen J 2008 Ballistic rectification in a Z-shaped graphene nanoribbon junction *Appl. Phys. Lett.* **92** 133119
- [29] Zhang L, Xue B and Wang Y 2019 Mode Conversion of the Edge Modes in the Graphene Double-Ribbon Bend *Materials (Basel)*. **12** 4008
- [30] Chen P-A, Chiang M-H and Hsu W-C 2017 All-zigzag graphene nanoribbons for planar interconnect application *J. Appl. Phys.* **122** 034301
- [31] Yang P, Tang Y, Yang H, Gong J, Liu Y, Zhao Y and Yu X 2013 Thermal management performance of bent graphene nanoribbons *RSC Adv.* **3** 17349–54
- [32] Pan C, He J, Yang D and Chen K 2016 Thermal Transport of Flexural and In-Plane Phonons Modulated by Bended Graphene Nanoribbons *J. Nanomater.* **2016** 1–7
- [33] Li K M, Xie Z X, Su K L, Luo W H and Zhang Y 2014 Ballistic thermoelectric properties in double-bend graphene nanoribbons *Phys. Lett. Sect. A Gen. At. Solid State Phys.* **378** 1383–7
- [34] Tran V-T T, Saint-Martin J, Dollfus P and Volz S 2017 Third nearest neighbor parameterized tight binding model for graphene nano-ribbons *AIP Adv.* **7** 075212
- [35] Wirtz L and Rubio A 2004 The phonon dispersion of graphite revisited *Solid State Commun.* **131** 141–52
- [36] Tran V-T, Saint-Martin J and Dollfus P 2015 High thermoelectric performance in graphene nanoribbons by graphene/BN interface engineering *Nanotechnology* **26** 495202
- [37] Saito R, Dresselhaus G, Dresselhaus M S D, Jorio A, Saito R, Dresselhaus G, Dresselhaus M S D and Jorio A 1998 *Physical Properties of Carbon Nanotubes* vol 3 (Imperial College Press)
- [38] Datta S 2000 Nanoscale device modeling: the Green's function method *Superlattices Microstruct.* **28** 253–78
- [39] Wu Y and Childs P A 2011 Conductance of Graphene Nanoribbon Junctions and the Tight Binding Model *Nanoscale Res. Lett.* **6** 1–5
- [40] Ozaki T, Nishio K and Kino H 2010 Efficient implementation of the nonequilibrium Green function method for electronic transport calculations *Phys. Rev. B* **81** 35116
- [41] Lewenkopf C H and Mucciolo E R 2013 The recursive Green's function method for graphene *J. Comput. Electron.* **12** 203–31

- [42] Do V-N 2014 Non-equilibrium Green function method: theory and application in simulation of nanometer electronic devices *Adv. Nat. Sci. Nanosci. Nanotechnol.* **5** 033001
- [43] D'Agosta R 2013 Towards a dynamical approach to the calculation of the figure of merit of thermoelectric nanoscale devices *Phys. Chem. Chem. Phys.* **15** 1758–65
- [44] Abraham Fedorovich Ioffe 1950 Energetic basis of thermoelectrical cells from semiconductors *Acad. Sci. USSR, Moscow* (in Russia)
- [45] Saiz-Bretín M, Malyshev A V., Domínguez-Adame F, Quigley D and Römer R A 2018 Lattice thermal conductivity of graphene nanostructures *Carbon N. Y.* **127** 64–9
- [46] Munrriz J, Domínguez-Adame F and Malyshev A V. 2011 Toward graphene-based quantum interference devices *Nanotechnology* **22**
- [47] Son Y-W, Cohen M L and Louie S G 2006 Energy Gaps in Graphene Nanoribbons *Phys. Rev. Lett.* **97** 216803